












Article

The Roles of Potassium and Calcium Currents in the Bistable Firing Transition

Fernando S. Borges ^{1,2}, Paulo R. Protachevicz ³, Diogo L. M. Souza ⁴, Conrado F. Bittencourt ⁴,
Enrique C. Gabrick ⁴, Lucas E. Bentivoglio ⁴, José D. Szezech, Jr. ^{4,5}, Antonio M. Batista ^{4,5},
Iberê L. Caldas ³, Salvador Dura-Bernal ^{1,6} and Rodrigo F. O. Pena ^{7,8,*}

- ¹ Department of Physiology and Pharmacology, State University of New York Downstate Health Sciences University, Brooklyn, NY 11203, USA
- ² Center for Mathematics, Computation and Cognition, Federal University of ABC, São Bernardo do Campo 09606-045, Brazil
- ³ Institute of Physics, University of São Paulo, São Paulo 05508-090, Brazil
- ⁴ Graduate Program in Science, State University of Ponta Grossa, Ponta Grossa 84010-330, Brazil
- ⁵ Department of Mathematics and Statistics, State University of Ponta Grossa, Ponta Grossa 84030-900, Brazil
- ⁶ Center for Biomedical Imaging and Neuromodulation, The Nathan S. Kline Institute for Psychiatric Research, Orangeburg, NY 10962, USA
- ⁷ Department of Biological Sciences, Florida Atlantic University, Jupiter, FL 33458, USA
- ⁸ Stiles-Nicholson Brain Institute, Florida Atlantic University, Jupiter, FL 33458, USA
- * Correspondence: penar@fau.edu

Abstract: Healthy brains display a wide range of firing patterns, from synchronized oscillations during slow-wave sleep to desynchronized firing during movement. These physiological activities coexist with periods of pathological hyperactivity in the epileptic brain, where neurons can fire in synchronized bursts. Most cortical neurons are pyramidal regular spiking (RS) cells with frequency adaptation and do not exhibit bursts in current-clamp experiments (in vitro). In this work, we investigate the transition mechanism of spike-to-burst patterns due to slow potassium and calcium currents, considering a conductance-based model of a cortical RS cell. The joint influence of potassium and calcium ion channels on high synchronous patterns is investigated for different synaptic couplings (g_{syn}) and external current inputs (I). Our results suggest that slow potassium currents play an important role in the emergence of high-synchronous activities, as well as in the spike-to-burst firing pattern transitions. This transition is related to the bistable dynamics of the neuronal network, where physiological asynchronous states coexist with pathological burst synchronization. The hysteresis curve of the coefficient of variation of the inter-spike interval demonstrates that a burst can be initiated by firing states with neuronal synchronization. Furthermore, we notice that high-threshold (I_L) and low-threshold (I_T) ion channels play a role in increasing and decreasing the parameter conditions (g_{syn} and I) in which bistable dynamics occur, respectively. For high values of I_L conductance, a synchronous burst appears when neurons are weakly coupled and receive more external input. On the other hand, when the conductance I_T increases, higher coupling and lower I are necessary to produce burst synchronization. In light of our results, we suggest that channel subtype-specific pharmacological interactions can be useful to induce transitions from pathological high bursting states to healthy states.

Keywords: ion channels; firing pattern transition; burst synchronization; bistability; hysteresis



Citation: Borges, F.S.; Protachevicz, P.R.; Souza, D.L.M.; Bittencourt, C.F.; Gabrick, E.C.; Bentivoglio, L.E.; Szezech, J.D., Jr.; Batista, A.M.; Caldas, I.L.; Dura-Bernal, S.; et al. The Roles of Potassium and Calcium Currents in the Bistable Firing Transition. *Brain Sci.* **2023**, *13*, 1347. <https://doi.org/10.3390/brainsci13091347>

Academic Editor: Gyorgy Lur

Received: 14 August 2023

Revised: 13 September 2023

Accepted: 15 September 2023

Published: 20 September 2023



Copyright: © 2023 by the authors. Licensee MDPI, Basel, Switzerland. This article is an open access article distributed under the terms and conditions of the Creative Commons Attribution (CC BY) license (<https://creativecommons.org/licenses/by/4.0/>).

1. Introduction

The classical Hodgkin–Huxley model, proposed in 1952, gave perspectives on understanding the electrical properties of neuronal dynamics considering the biophysical mechanics of the exchange of charges by sodium and potassium ion channels [1,2]. Nowadays, much more is known about the variety of channels involved in the neuronal machinery [3,4]

and their relation to healthy brain function [5,6] and diseases [7,8]. Despite that, the complete understanding of the role of such ion channels is still inciting many research questions in this matter [9,10]. Currently, an extensive perspective of research considering the neuroinformatics approach provides new insights into understanding and treating brain diseases [11,12]. Neuroinformatics has been used to fit and explore the dynamics of realistic neuron activities [13], including the influence of ion channels [14] and different currents to which neurons can be exposed [15,16]. In the present work, we are particularly interested in the ion channel influence as an adaptive mechanism that affects the firing pattern and synchronization transitions since adaptation plays an important role in synchronization [17,18].

The transition of neuronal single-cell firing patterns can emerge as a sum of different sources. In this framework, topology properties, such as the number [18,19], the type [20], the intensity of neuronal interactions [21–25], and the time delay of chemical transmission [26,27], can contribute to the firing patterns transitions. Besides that, noise input currents, as well as external perturbations, can also play a role in the spike and burst transitions [28–30]. The relationship between how single spikes and bursts are maintained in relation to theta and gamma oscillations was recently discovered [31]. However, beyond the topology factors, intrinsic neuronal properties have been pointed out as the main factor in firing pattern transitions [32,33]. For example, the mechanism of the adaptation of excitability appears to be a key factor in the transition between spike and burst patterns [34,35]. Typically, spike adaptation corresponds to the capability of neurons to reduce their spike frequency due to recent sub and over-threshold neuronal activities [36–38]. It is also known that potassium and calcium currents develop a role in neuronal adaptation mechanisms [39–41].

The emergence of different network firing patterns is mainly associated with the intrinsic properties of the neurons, for example, ion channel density [33,42] and type [43,44], as well as the synaptic input currents [45,46], noise [47,48], and other kinds of couplings and external inputs that the neurons of the network can submit [49]. A particular type of populational neuronal firing pattern in network dynamics is the synchronized state. In this context, the influence of the ion channels in synchronization was demonstrated by Boaretto et al. It was shown that small changes in ionic conductance can affect the capacity of the networks to exhibit phase synchronization [50]. Landenbauer et al. studied the impact of adaptation on synchronization by comparing coupled neuronal models, and highlighting the importance of the comprehension of such a mechanism on the emergence of the network dynamics [51]. Synchronized activities are essential for the correct functioning of the brain; however, highly synchronized activities with burst firing patterns are associated with epileptic seizures [52]. Besides the high synchronization levels, epileptic activities can also be related to burst firing patterns [53,54] and low synaptic inhibition [55]. The experimental results of cultured neuronal networks, based on multi-electrode arrays, indicated that burst activities present stronger synchrony capabilities with a sufficient level of excitation [56]. These currents are also known to develop frequency-dependent resonant mechanisms, an example being the hyperpolarization-activated I_h current, which is related to K^+ and connected to theta resonance and the T-type voltage-dependent Ca^{2+} channel that acts as an amplifier [57]. In addition, T-type channels are related to the increase in burst activities in seizure generation [58] and have been identified to play a central role in epileptogenesis in the pilocarpine model of epilepsy [59]. Besides that, after status epilepticus, the density of T-type Ca^{2+} channels was upregulated in pyramidal neurons [60]. However, a deeper understanding of the complementary roles of channels in the complex firing patterns of neurons and networks has yet to be uncovered.

Bistable patterns are dynamic behaviors that can be exhibited from the levels of a single neuron [61] to a network [62,63]. Bistability in synchronization emerges as a collective dynamic interplay between excitatory and inhibitory interactions between neurons [64]. Recently, Akcay et al. reported that bistability with different phases can emerge in a pair of Type I neurons connected by chemical synapses [65], a phenomenon related to the

history dependency of the system and known as hysteresis. Bistability and hysteresis are two mechanisms that can be associated with the emergence of burst oscillations [66]. In cortical neurons, the state-dependent coexistence of tonic and burst firings gathers the conditions for the emergence of bistability and hysteresis [67]. Simplified neuronal and oscillator models have reported the emergence of bistable firing patterns [34,68]. Bistable and multi-stable dynamics are said to play a role in both healthy [69] and abnormal brain activities [70]. For this reason, studying a detailed description of ion channels in biophysical neuronal models can bring new light to understanding such firing patterns that emerge in brain activities.

The main purpose of this work is to investigate the impact of potassium and calcium currents as an adaptive mechanism that enables the emergence of burst synchronization associated with a bistable regime [34]. In our simulations, burst activities emerge with highly synchronized firing patterns for a range of synaptic couplings (g_{syn}) and external current input (I). Slow potassium currents promote the emergence of high-synchronous activities and spike-to-burst firing pattern transitions. This transition is bistable where physiological asynchronous states coexist with pathological burst synchronization. The hysteresis curve of the coefficient of variation of the inter-spike interval demonstrates that a burst can be initiated by synchronized firing states; however, asynchronous states result in an asynchronous spike firing pattern. Furthermore, we notice that for high values of high-threshold (I_L) conductance, a synchronous burst appears when neurons are weakly coupled and receive more external input. On the other hand, when the conductance I_T increases, the opposite is observed. As our main conclusions, we show how the dynamic and biophysical characteristics of the slow potassium and calcium currents in networks promote bistable transitions. We believe that this work has the potential to uncover pharmacological targets in a manner in which high synchronization can be efficiently hindered.

Our paper is organized as follows. In Section 2, we describe the fundamental equations that govern the dynamics of the model and the diagnostics considered for the analysis of neuronal dynamics. In Section 3, we present our results. We depict the neuronal dynamics by first presenting the perspective of a single network and, following that, presenting the network configuration. We gradually introduce the role of potassium and calcium currents by observing how the emergence of the bistable regime takes place. Finally, in Section 4, we present our discussion to expose our future perspectives and conclusions of this work.

2. Materials and Methods

2.1. Neural Model

We consider a conductance-based model in which the membrane potential V [71] is given by the following equation:

$$C_m \frac{dV}{dt} = -g_{\text{leak}}(V - E_{\text{leak}}) - I_{\text{ionic}}, \quad (1)$$

where $C_m = 1 \mu\text{F}/\text{cm}^2$ is the specific capacitance of the membrane, g_{leak} is the resting membrane conductance, E_{leak} the reversal potential, and I_{ionic} is the sum of partial ionic currents I_j . The voltage-dependent ionic currents have the same general equation:

$$I_j = g_j m^M h^N (V - E_j), \quad (2)$$

where the j -th ionic current I_j is expressed as the product of the maximum conductance of each ion j with the conductance g_j of the respective ion. The variables m and n are the activation variables of sodium and potassium, respectively, and h is the inactivation variable of the sodium ion channel [1]. The difference between the membrane potential V and the reversal potential for a specific ion E_j is $(V - E_j)$ [71].

2.2. Description of Ionic Currents

The total ionic current I_{ionic} described in Equation (1) is given by:

$$I_{\text{ionic}} = I_{\text{Na}} + I_{\text{K}} + I_{\text{M}} + I_{\text{L}} + I_{\text{T}}, \quad (3)$$

where I_{Na} and I_{K} are the basic sodium and potassium currents of the Hodgkin–Huxley model [72], I_{M} is a slow voltage-dependent potassium current responsible for spike frequency adaptation [73], I_{L} is a high-threshold calcium current, and I_{T} is a low-threshold calcium current [74,75].

2.2.1. Sodium and Potassium Currents

The voltage-dependent sodium and potassium currents are described by the Hodgkin–Huxley equations and were adapted for central neurons by Traub and Miles [72]. The sodium currents are described in the following equations:

$$\begin{aligned} I_{\text{Na}} &= g_{\text{Na}} m^3 h (V - E_{\text{Na}}), \\ \frac{dm}{dt} &= \alpha_m(V)(1 - m) - \beta_m(V)m, \\ \frac{dh}{dt} &= \alpha_h(V)(1 - h) - \beta_h(V)h, \\ \alpha_m &= \frac{-0.32(V - V_{\text{T}} - 13)}{\exp[-(V - V_{\text{T}} - 13)/4] - 1}, \\ \beta_m &= \frac{0.28(V - V_{\text{T}} - 40)}{\exp[(V - V_{\text{T}} - 40)/5] - 1}, \\ \alpha_h &= 0.128 \exp[-(V - V_{\text{T}} - 17)/18], \\ \beta_h &= \frac{4}{1 + \exp[-(V - V_{\text{T}} - 40)/5]}, \end{aligned} \quad (4)$$

and the potassium currents are described by

$$\begin{aligned} I_{\text{K}} &= g_{\text{K}} n^4 (V - E_{\text{K}}), \\ \frac{dn}{dt} &= \alpha_n(V)(1 - n) - \beta_n(V)n, \\ \alpha_n &= \frac{-0.032(V - V_{\text{T}} - 15)}{\exp[-(V - V_{\text{T}} - 15)/5] - 1}, \\ \beta_n &= 0.5 \exp[-(V - V_{\text{T}} - 10)/40]. \end{aligned} \quad (5)$$

The conductance of sodium and potassium are $g_{\text{Na}} = 50 \text{ mS/cm}^2$, $g_{\text{K}} = 5 \text{ mS/cm}^2$, and the reversal potentials are $E_{\text{Na}} = 50 \text{ mV}$, $E_{\text{K}} = -100 \text{ mV}$, respectively. The V_{T} variable is used to adjust the peak threshold in our simulations: $V_{\text{T}} = -55 \text{ mV}$.

2.2.2. Slow Potassium Current

The non-inactivating slow current of potassium ions is described by the equations:

$$\begin{aligned} I_{\text{M}} &= g_{\text{M}} p (V - E_{\text{K}}), \\ \frac{dp}{dt} &= (p_{\infty}(V) - p) / \tau_p(V), \\ p_{\infty}(V) &= \frac{1}{1 + \exp[-(V + 35)/10]}, \\ \tau_p(V) &= \frac{\tau_{\text{max}}}{3.3 \exp[(V + 35)/20] + \exp[-(V + 35)/20]}, \end{aligned} \quad (6)$$

$$\tau_p(V) = \frac{\tau_{\text{max}}}{3.3 \exp[(V + 35)/20] + \exp[-(V + 35)/20]} \quad (7)$$

where $g_{\text{M}} = 0.03 \text{ mS/cm}^2$ and $\tau_{\text{max}} = 1000 \text{ ms}$ [40,73].

2.2.3. Calcium Currents

The first calcium current used to produce bursting is due to a high-threshold Ca^{2+} current (I_L , L-type, and long-lasting current) and is described as:

$$\begin{aligned}
 I_L &= g_L q^2 r (V - E_{\text{Ca}}), \\
 \frac{dq}{dt} &= \alpha_q (V) (1 - q) - \beta_q (V) q, \\
 \frac{dr}{dt} &= \alpha_r (V) (1 - r) \beta_r (V) r, \\
 \alpha_q &= \frac{0.055 (-27 - V)}{\exp[(-27 - V)/3.8] - 1}, \\
 \beta_q &= 0.94 \exp[(-75 - V)/17], \\
 \alpha_r &= 0.000457 \exp[(-13 - V)/50], \\
 \beta_r &= \frac{0.0065}{\exp[(-15 - V)/28] + 1},
 \end{aligned} \tag{8}$$

where the maximum conductance of I_L is $g_L = 0.3 \text{ mS/cm}^2$ [75].

The equations for the second type of calcium current, the low-threshold Ca^{2+} current (I_T , T-type, transient current), are:

$$\begin{aligned}
 I_T &= g_T s_\infty^2 u (V - E_{\text{Ca}}), \\
 \frac{du}{dt} &= (u_\infty (V) - u) / \tau_u (V), \\
 s_\infty (V) &= \frac{1}{1 + \exp[-(V + V_x + 57)/6.2]}, \\
 u_\infty (V) &= \frac{1}{1 + \exp[(V + V_x + 81)/4]}, \\
 \tau_u (V) &= 30.8 + \frac{(211.4 + \exp[(V + V_x + 113.2)/5])}{(1 + \exp[(V + V_x + 84)/3.2])},
 \end{aligned} \tag{9}$$

where $g_T = 0.4 \text{ mS/cm}^2$ is the maximal conductance of the low-threshold calcium current, and $V_x = 2 \text{ mV}$ is a uniform shift of the voltage dependence [76,77].

Calcium currents change intracellular calcium concentration $[\text{Ca}^{2+}]_i$, and as a consequence, the potential reversal of calcium ions (E_{Ca}), which is given by

$$E_{\text{Ca}} = \frac{RT}{2F} \times \log \left(\frac{[\text{Ca}^{2+}]_o}{[\text{Ca}^{2+}]_i} \right), \tag{10}$$

where $R = 8.31 \text{ J K}^{-1} \text{ mol}^{-1}$ is the universal gas constant, $T = 309.15 \text{ K}$ is the temperature, and $F = 96485 \text{ C mol}^{-1}$ is the Faraday constant. The dynamics of the calcium concentration is given by

$$\frac{d[\text{Ca}^{2+}]_i}{dt} = \frac{-5.0(I_L + I_T)}{Fd} + \frac{([\text{Ca}^{2+}]_\infty - [\text{Ca}^{2+}]_i)}{\tau_r}, \tag{11}$$

where $[\text{Ca}^{2+}]_i$ is the intracellular Ca^{2+} concentration, $[\text{Ca}^{2+}]_o = 2.0 \text{ mM}$ is the extracellular Ca^{2+} concentration, $[\text{Ca}^{2+}]_\infty$ is the maximum concentration of calcium inside the cell, $d = 1 \text{ }\mu\text{m}$ and $\tau_r = 5 \text{ ms}$.

2.2.4. Neuronal Network

We consider a randomly connected neuronal network composed of Hodgkin–Huxley neurons described in the previous sections, where the neurons are 80% excitatory and 20% inhibitory [78]. We consider an Erdős–Rényi network with a connection probability $p = 0.1$,

and there are no auto-connections [79]. For the representation of each neuron i in a network, Equation (1) with the addition of synaptic connections is represented by

$$C_m A \frac{dV_i}{dt} = A(-g_{\text{leak}}(V_i - E_{\text{leak}}) - I_{\text{ionic}}^i + I_{\text{syn}}^i) + I, \quad (12)$$

where V_i represents the membrane potential, I_{ionic}^i corresponds to the ion currents, I is a constant current that is the same for all neurons, and $A = 0.2895 \times 10^{-3} \text{ cm}^2$ represents the membrane area. The neuron area taken as a cylinder is given by $A = \pi dL$, with $d = L = 0.0096 \text{ cm}$ [40]. The specific capacitance of the membrane is $C_m = 1 \text{ } \mu\text{F}/\text{cm}^2$; therefore, the total capacitance is $0.2895 \times 10^{-3} \text{ } \mu\text{F}$. All the terms in Equation (12) have units of current (μA). The parameters g_{leak} , g_{Na} , g_{K} , g_{M} , g_{L} , g_{T} , and g_{syn} are density conductances with mS/cm^2 as the unit.

The chemical synaptic current that arrives in the neuron i is represented by

$$I_{\text{syn}}^i = \sum_{k=1}^N (V_{\text{rev}}^k - V_i) M_{ik} g_k, \quad (13)$$

where V_{rev}^i represents the synaptic reversal potential, M is the adjacency matrix of the connections, and g_k is the synaptic conductance from the neuron k . V_{rev}^i assumes a value equal to $V_{\text{rev}}^i = V_{\text{rev}}^{\text{exc}} = 0 \text{ mV}$ for excitatory and $V_{\text{rev}}^i = V_{\text{rev}}^{\text{inh}} = -80 \text{ mV}$ for inhibitory synaptic connection from the neuron k . The adjacency matrix is composed of element M_{ij} equal to 1 to represent connections from neuron k to neuron i , and equal to 0 to represent the absence of such a connection. g_k is updated in the time of neuron k overpass $V = 0$ with a positive potential derivative ($dV/dt > 0$). The time of spikes of a certain neuron k , denoted as t_k , is also defined by these two conditions in the membrane potential. In this way, the update in synaptic conductance is represented by $g_k \rightarrow g_k + g_{\text{syn}}$, where g_{syn} is the chemical intensity of the synaptic updates, the same for excitatory and inhibitory connections. In addition to the update rule due to spiking, each synaptic conductance g_k evolves by an exponential decay described by $dg_k/dt = -g_k/\tau_{\text{syn}}$ with $\tau_{\text{syn}} = 5.0 \text{ ms}$.

2.3. Measures

2.3.1. Firing Rate

We calculate the mean firing rate (in Hz) of all neurons in the network by

$$F = \frac{1}{N} \sum_{i=1}^N \left(\frac{1}{T} \int_0^T \delta(t - t_i) dt \right), \quad (14)$$

where t_i is the time of the i -th spike, $N = 1000$ is the number of neurons, and $T = 5 \text{ s}$ is the time window considered for the analyses.

2.3.2. Coefficient of Variation

We use the inter-spike intervals (ISIs), where the i -th interval is defined as the difference between two consecutive spike times t_{i+1} and t_i , namely $\text{ISI}_i = t_{i+1} - t_i > 0$. From the ISI series, the first interval is referred to as ISI_1 followed by the subsequent intervals, namely $\text{ISI}_2, \text{ISI}_3, \dots$, and ISI_n . The ratio between the standard deviation and the mean (indicated by $\langle \cdot \rangle$) gives rise to the coefficient of variation

$$\text{CV}_i = \frac{\sqrt{\langle (\text{ISI}_i - \langle \text{ISI}_i \rangle)^2 \rangle}}{\langle \text{ISI}_i \rangle}, \quad (15)$$

for the i -th neuron. Finally, the average of CV_i over all neurons is given by

$$\text{CV} = \frac{1}{N} \sum_{i=1}^N \text{CV}_i. \quad (16)$$

2.3.3. Synchronization

To measure the level of synchronization exhibited by the neuronal network, we consider the complex order parameter of Kuramoto [80] given by

$$\rho(t) = \left| \frac{1}{N} \sum_{j=1}^N \exp[i\Psi_j(t)] \right|, \quad (17)$$

where the phase of each neuron j is represented by

$$\Psi_j(t) = 2\pi \frac{t - t_{j,m}}{t_{j,m+1} - t_{j,m}}. \quad (18)$$

where $t_{j,m}$ represents the m -th spikes of the neuron j . The time t of the parameter is defined in the interval $t_{j,m} < t < t_{j,m+1}$. The time-average order parameter is calculated by

$$R = \frac{1}{t_{\text{fin}} - t_{\text{ini}}} \int_{t_{\text{ini}}}^{t_{\text{fin}}} \rho(t) dt, \quad (19)$$

where t_{ini} and t_{fin} represent the initial and final times for the analyses of synchronization in the neuronal network [81].

The implementation of the numerical simulations was performed using self-developed C and NetPyNE codes [82] and can be freely accessed in <https://github.com/FernandoSBorges/BistabilityHH> (accessed on 1 September 2023).

3. Results

3.1. Neuron Dynamics

We begin by presenting some essential dynamical characteristics of the neurons and networks. Figure 1 displays the biophysical properties of neurons and their dependence on the ionic conductance of the slow potassium M-current, and Figure 2 displays the additional presence of calcium currents.

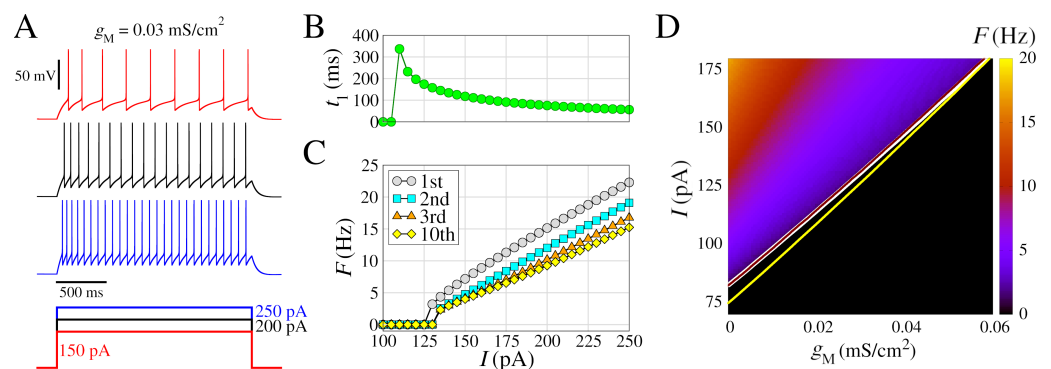


Figure 1. Model of regular spiking neuron, with I_{Na} and I_{K} for spike generation, and slow K⁺ current (I_{M}) for spike frequency adaptation. (A) (Top) Voltage traces with different amplitudes of the depolarizing pulses (bottom), $V = -85 \text{ mV}$ before the depolarizing pulses. (B) Time to first spike (t_1) as a function of the injected current (amplitude of the pulse I). (C) Frequency–current curves (F/I), where the instantaneous firing rate (inverse of the inter-spike interval) is represented as a function of I . The curves indicated by different colors correspond to the 1st, the 2nd, the 3rd, and the 10th spikes in the train. (D) Spike frequency F (in color) as function of g_{M} and I , considering 5.0 s time window. The white line represents the transition where $F > 0$ for $g_{\text{T}} = 0$ and $g_{\text{L}} = 0$. Additionally, this transition lines for $g_{\text{T}} = 0$ and $g_{\text{L}} = 0.1 \text{ mS/cm}^2$ (brown line), and $g_{\text{T}} = 0.4 \text{ mS/cm}^2$ and $g_{\text{L}} = 0$ (yellow line) are shown. Other parameters are $L = d = 96.0 \text{ }\mu\text{m}$, $g_{\text{leak}} = 0.01 \text{ mS/cm}^2$, $E_{\text{leak}} = -85.0 \text{ mV}$, $g_{\text{Na}} = 50 \text{ mS/cm}^2$, $V_{\text{T}} = -55.0 \text{ mV}$, $g_{\text{K}} = 5 \text{ mS/cm}^2$, $\tau_{\text{max}} = 1000 \text{ ms}$, and $g_{\text{M}} = 0.03 \text{ mS/cm}^2$. The absolute values of the membrane potential of (A) are available at <https://github.com/FernandoSBorges/BistabilityHH> (accessed on 1 September 2023).

In Figure 1, we present extended characteristics for the regular spiking model by changing the input amplitudes. This model includes I_{Na} and I_K for the generation of spikes, and slow K^+ current (I_M) for the adaptation of the spike frequency. The frequency of the action potentials increases with the input amplitude as shown by the three exemplar voltage traces (Figure 1A). For input amplitudes of $I = 110$ pA, the neuron exhibits a single spike after ≈ 350 ms from the start of stimulus (Figure 1B). The second spike occurs for $I = 130$ pA, where the first frequency F is obtained by $1/ISI_1$. Regular spiking behavior is observed for $I > 135$ pA (Figure 1C). As the amplitude increases, no bursting appears but rather a linear increase in frequency with progressively lower frequencies for each spike in the train as a consequence of the adaptation mechanism (Figure 1C).

In Figure 1D, we show F (in color) as a function of g_M and I , where F (Equation (14)) is calculated considering spikes in a time window of 5.0 s. The g_M has a great influence on the way the neuron fires by changing the minimum value of I , where $F > 0$ (white line), and in addition, higher values of g_M have lower values of F for the same value of I . This shows that the slow K^+ current (I_M), related to the adaptation of the spike frequency, has a strong influence on the response of the neuronal firing to external stimuli. On the other hand, low-threshold calcium currents (I_T) have low alterations in F (yellow line), and high-threshold calcium currents (I_L) have an almost null effect (brown line).

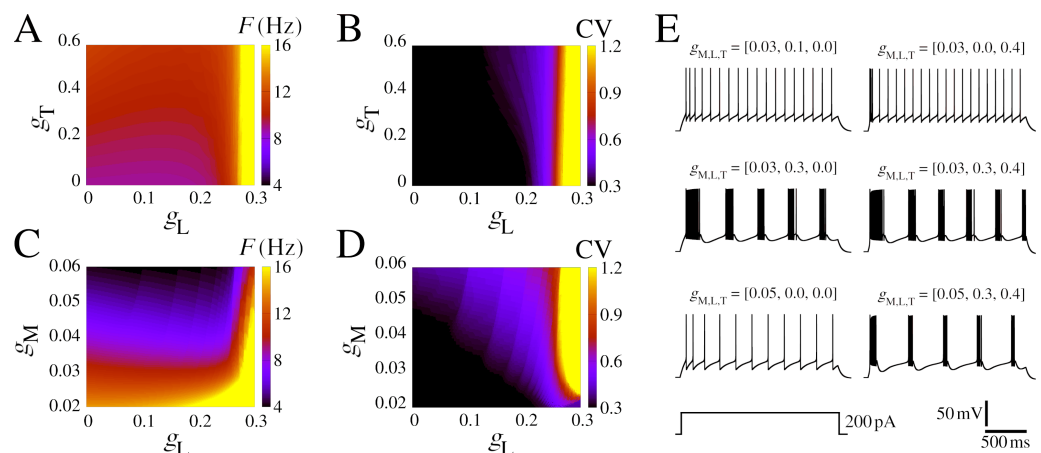


Figure 2. Firing pattern for different I_M , I_T , and I_L conductances. (A) Firing rate in colored (g_T , g_L)-diagram for $g_M = 0.03$ mS/cm². (B) The same as (A) for the CV. (C) Firing rate in colored (g_M , g_L)-diagram for $g_T = 0.4$ mS/cm². (D) The same as (C) for the CV. (E) Exemplar voltage traces considering different values of g_M , g_L , and g_T , where each parameter combination is shown atop and $V = -85$ mV before the depolarizing pulses. Other parameters are the same as Figure 1 with $I = 200$ pA.

In order to understand the role of calcium currents in the neuron model, we show some diagrams that vary the low-threshold (g_T) and high-threshold (g_L) conductances. We delimited the range of the parameter based on the firing rate values lower than 20 Hz. Figure 2A–D display colored (g_T , g_L) and (g_M , g_L)-diagrams for F and CV. Figure 2E exhibits some examples of selected simulations. The initial burst extends into sustained bursting due to the influence of high-threshold Ca^{2+} ; this phenomenon becomes evident for $g_L > 0.026$ mS/cm² (Figure 2B). This observed frequency remains below 12 Hz for $g_M > 0.03$ mS/cm² and $g_L < 0.025$ mS/cm² (Figure 2C), which is typically found in neurons in the rat somatosensory cortex [83]. The coefficient of variation (CV) undergoes a transition from 0.3 to >1.0 depending on the value of g_L for $g_M > 0.022$ mS/cm². This CV transition is abrupt and occurs at approximately $g_L \approx 0.25$ mS/cm² (Figure 2D). The two main effects of increasing g_T are a reduction in the time to the first spike and to generate the initial bursting pattern (Figures 2E and S1). For some values of the g_L and g_M combination, regular bursts appear. Furthermore, the amplitude of the input current is also responsible for the change in the area in which regular burst activity ($CV > 1.0$) is observed in the colored diagram. Higher values of I increase the minimum g_M values to have bursts, for

$I = 200$ pA the minimum $g_M = 0.022$ mS/cm², while for $I = 250$ pA, $g_M > 0.038$ mS/cm² is necessary (Figure S2).

The panels in Figure 2 provide clear evidence of the impact of adaptation and burst development resulting from the influence of slow potassium and calcium currents. In the next section, we will move forward with the network effects.

3.2. Neuron Networks

Next, we study the behavior of networks of neurons, such as the ones discussed above, connected via chemical synapses. As such, the type of behavior varies depending on the input current I and the strength of the synapses g_{syn} . A highly interesting phenomenon that arises in the network spiking pattern is the transition from asynchronous spiking to burst synchronization. Moreover, in this transition, bistable firing patterns are observed, where both asynchronous and synchronous states coexist.

In Figure 3, we present a systematic study of the parameter combinations of constant applied current and the chemical synaptic conductance (I and g_{syn}) in the measures F , CV, and R (see Section 2.3). These measures are displayed, respectively, in Figure 3A–C. Notice that here, we purposely remove the effect of $g_{M,L,T}$ to show that without the slow potassium and calcium currents, there is no burst no matter the input amplitude and coupling (Figure 3B). Moreover, the firing rate increases with I and g_{syn} (Figure 3A). Interestingly, however, as seen in Figure 3C,D, even without the effect of $g_{M,L,T}$, the raster plot shows a synchronized behavior with activity around 4 Hz due to population dynamics. This is noticed for combined low values of input current I and g_{syn} , whereas for higher values, only asynchronous behavior is observed (Figure 3E).

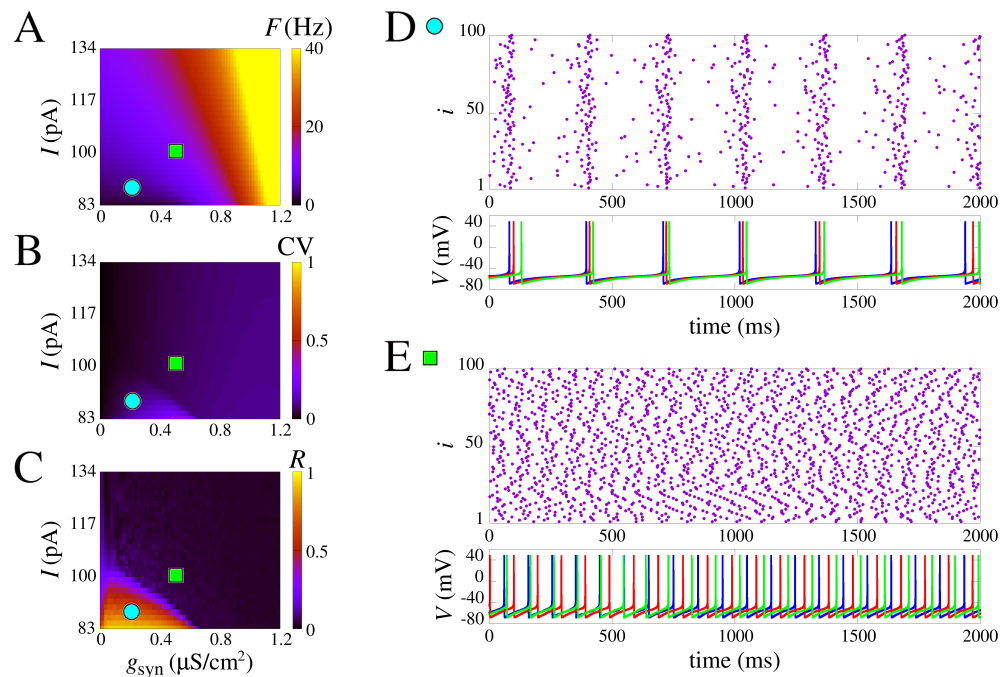


Figure 3. Spike synchronization in space parameters as a function of I and synaptic conductance (g_{syn}). (A) Mean firing frequency. (B) Coefficient of variation, and (C) mean order parameter. (D,E) Raster plot and the neuronal membrane potentials for the parameter indicated in (A–C). (D) Synchronized spikes for the parameters $I = 88.3$ pA and $g_{syn} = 0.2$ μ S/cm². (E) Desynchronized spikes for the parameters $I = 98.9$ pA and $g_{syn} = 0.5$ μ S/cm². We use the model without slow potassium and calcium currents, i.e., $g_{M,L,T} = [0, 0, 0]$.

The results demonstrate that the lack of slow potassium and calcium currents hinders the possibility of observing single-cell bursting, even in a network. Transitions from asynchronous to synchronous activity are still present as seen in how the circle and square

are in areas of different values of R in Figure 3C, but the CV changes are slight and nearly absent, indicating only spikes.

3.3. Bistable Regime

The results are different when the effect of the slow potassium current is added. As shown in Figure 4, increasing g_{syn} results in transitions from asynchronous activity to a burst synchronization. Noticeably, the voltage traces exhibit individual bursting for neurons with a regular spike firing pattern without coupling. These network bursts are observed for fixed values of $I < 200.0$ pA and $g_{\text{syn}} > 1.0$ $\mu\text{S}/\text{cm}^2$.

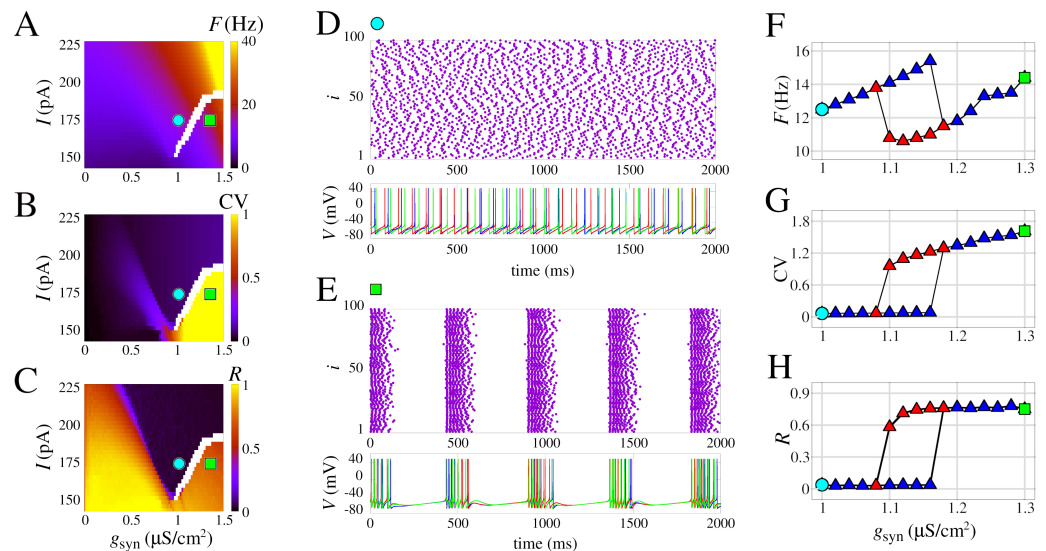


Figure 4. Burst synchronization in space parameters as a function of I and chemical synaptic conductance (g_{syn}). (A) Mean firing frequency. (B) Coefficient of variation. (C) Mean order parameter. (D,E) Raster plot and the neuronal membrane potentials for the parameter indicated in (A–C). (D) Desynchronized spikes for the parameters $I = 170.4$ pA and $g_{\text{syn}} = 1$ $\mu\text{S}/\text{cm}^2$ are observed and synchronized bursts are shown for the parameters $I = 170.4$ pA and $g_{\text{syn}} = 1.3$ $\mu\text{S}/\text{cm}^2$ in (E). (F–H) Curves of F , CV , and R , respectively, for increasing values of g_{syn} (blue triangles) and decreasing values of g_{syn} (red triangles). We use the model with slow potassium and without calcium currents, i.e., $g_{\text{M,L,T}} = [0.03, 0, 0]$ mS/cm².

The emergence of the bursting synchronization by increasing values of g_{syn} has a marked effect on the measures F , CV , and R . When $I = 170.4$ pA, this sudden increase that leads to the transition starts approximately at $g_{\text{syn}} = 1.09$ $\mu\text{S}/\text{cm}^2$ for initial conditions with asynchronous spikes, and $g_{\text{syn}} = 1.18$ $\mu\text{S}/\text{cm}^2$ for initial conditions with burst synchronization. This hysteresis is indicated in the white area in Figure 4A–C and is an observation that is a strong indication of bistability. Figure 4D shows a raster plot and voltage traces for the asynchronous spike pattern, and Figure 4E shows the same for burst synchronization. A comparison of the blue and red curves in Figure 4F–H shows the exact transition area from asynchronous activity to bursting synchronization.

The results demonstrate that the slow potassium current (here considered as $g_{\text{M}} = 0.03$ mS/cm²) can promote bistable dynamics in neuronal networks. This type of observation related to a biophysically grounded parameter is a key factor in understanding how bistability relates to other brain phenomena, such as decision making or pathologies such as epilepsy. The transition from spike to network burst was observed in [18] for the adaptive exponential integrate-and-fire neuron model, and, later, bistability in neuronal networks using this simple neuron model was related to epileptic seizures elsewhere [34,84].

3.4. Calcium Effects in the Bistability

We showed that a slow potassium current is necessary to observe bistability. A natural question that arises from our work is how the firing transition and the bistable dynamics depend on the single-cell calcium ionic channels. In this section, we discuss how quantitative changes emerge for different combinations of calcium currents. Figure 5 shows how CV values depend on constant current and chemical synaptic conductance (I, g_{syn}) with respect to different values of $g_{\text{M,L,T}}$. The bistable parameter region is identified in white and separate black and reddish/blueish regions for asynchronous spikes (low CV) to synchronous bursts (high CV), respectively. Figure S3 demonstrates that these qualitative patterns are maintained for the firing frequency F and the mean order parameter R .

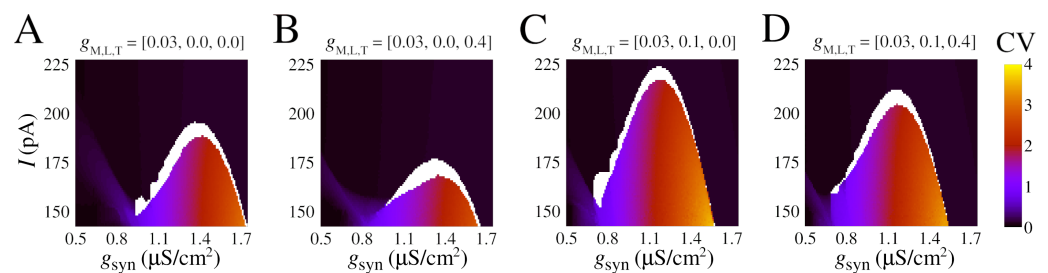


Figure 5. Effect of calcium currents in the burst synchronization in space parameters as a function of input current (I) and chemical synaptic conductance (g_{syn}). (A–D) Coefficient of variation (CV) for different combinations of $g_{\text{M,L,T}}$ (see values atop). (A) Model with slow potassium and without calcium currents, the same parameters of Figure 4. (B) Model with slow potassium and only low-threshold calcium current (I_{T}). (C) Model with slow potassium and only high-threshold calcium current (I_{L}). (D) Model with slow potassium and both low-threshold and high-threshold calcium currents (I_{T} and I_{L}).

Indeed, the transition area changes according to the presence of ionic currents. The parameters g_{syn} and I are sensitive to changes with respect to $g_{\text{M,L,T}}$. In particular, high-threshold calcium, controlled by g_{L} , is the one that causes a greater change by allowing transitions at lower values of the g_{syn} (Figure 5C). Furthermore, the synchronous area (reddish/blueish) is larger for the high-threshold calcium change, allowing for burst synchronization for $I > 200.0$ pA. In contrast, low-threshold calcium promotes the opposite effect by slightly increasing the value of g_{syn} necessary to observe a transition (compare Figure 5A,B and Figure 5C,D). Figure S4 shows the dynamic behavior of currents generated by each active conductance in a neuron during the bistable regime. The analysis includes the total synaptic current (I_{syn}), the total ionic current (I_{ionic}), the fraction of outward ionic currents, and the fraction of inward ionic currents. See [85] for a detailed analysis of currents in neural models with different conductance densities.

Our results show that calcium has a double effect in promoting the bistability of asynchronous/synchronous activity that we observed: it can either facilitate it by allowing lower values of g_{syn} to act on the transition when the high-threshold calcium channel is used or make it harder via an opposite effect mediated by the low-threshold calcium channel.

4. Discussion and Conclusions

In this work, we extend the analysis of bistable firing transitions in neurons and networks [34,61–63] considering the effect of potassium and calcium currents. To quantify these firing patterns, we employ the usual measures, including the firing rate, CV, and synchronization level. This provides an important link to the role of these ionic currents in controlling the network behavior. We notice that in the absence of the joint effect of potassium and calcium, there is only a spike synchronization pattern, and bursts at the single-cell level are not observed. In the presence of slow potassium and calcium currents, bistability is identified by hysteresis among synchronized bursting and asynchronous activity. It is worth noting a significant distinction from the study conducted by [34], which

utilized the adaptive exponential integrate-and-fire neuron model. In our current model, we not only observe the effects but also establish a direct link to the underlying neurobiology, enabling us to propose experimental interventions that can be tested empirically through the manipulation of ionic currents.

Different voltage-dependent ion channels are responsible for the control of excitability and can play an intrinsic role in pathologies, such as epilepsy [86–88], Parkinson's [89], and Alzheimer's disease [90]. In particular, potassium and calcium ions have been found to play a role in many of these diseases [91–93]. In addition, some research has evidenced that blocking such ion channels can play a role in avoiding the mechanism associated with the emergence of epileptic activities [94]. Detailed investigations have been devoted to identifying the variations and mutations of calcium and potassium ion channels that exert the most influence on epileptic activity [95].

The opening and closing of such ion channels can have different effects on neuronal excitability. The majority of potassium ion channels open when the membrane depolarizes and close when it hyperpolarizes. The M current, in particular, acts in the subthreshold domain and limits the ability of the neuron to fire repetitively [96]. Their involvement in epileptic activities is still being investigated [97,98], and some recent research studying the lost- and gain-of-function of such ions has started to clarify these issues [2,99]. Besides that, mutations in potassium channels have also been identified as an important factor in the parthenogenesis of human epilepsy [100]. Such mutations and anomalies can be generated by external factors, e.g., the use of drug substances that have evidenced potential for changing the expression of potassium channels [101]. Recently, precise studies and therapies have focused on the mutation of potassium channel genes [102]. It is clearly important to further investigate how channel-blocking mechanisms can serve to control network activity [103,104].

Regarding calcium, we have shown that neurons embedded with these channels can exhibit a spike-to-burst transition [105]. In particular, two types of calcium currents are highlighted: L-type and T-type. The former, where “L” stands for large or long-lasting, is a high-voltage activated channel. The latter, where “T” stands for transient, is a low-voltage activated channel. Calcium currents are highly involved in network high synchronous patterns that are observed in epileptic seizures [106]. Not surprisingly, calcium channel blockers may act as anti-seizure drugs for prevention and treatment [107,108], i.e., the blocking of such ion channels can attenuate the burst firing pattern [109] and hinders epileptic depolarization [110]. Nonetheless, it is challenging to develop drugs that are subtype-specific, and in most cases, they have not been developed yet [111]. Thus, understanding the spike-to-burst pattern through computer simulations and neuroinformatics has the potential to elucidate the emergence of synchronous patterns related to epileptic activities [112]. A combined treatment using calcium channels blockers was demonstrated to be beneficial in anticonvulsant and antinociceptive effects [113] (for the reader interested in channel blockers, please see the list in [111]). According to our results, whereas L-type channels make transitions easier by lowering the value of synaptic strength (g_{syn}) necessary for the transition, T-type channels have the opposite effect.

Admittedly, there is yet a joint effect of potassium and calcium currents that we have not addressed in our simulations, which is the one provided by Ca^{2+} -dependent K^+ currents ($I_{K(Ca)}$) [114–116]. These potassium currents, influenced by calcium concentration, are known to induce prolonged hyperpolarization pauses, thereby significantly impacting the firing properties of neurons. The exploration of their intricate behavior is a key aspect of our future research plans. In future work, we will also analyze the effect of the hyperpolarization-activated cation current (I_h) [117] and the persistent Na^+ current [118] on the bistability.

Our results also extend the current knowledge of the joint effect of calcium and potassium ion channels in the context of other important firing pattern transitions. Based on our analysis, we can predict the ionic blockers required to avoid and treat high synchronous activity. These blockers would change the single-cell bursts that may result in epileptic

seizures to asynchronous activity. In particular, we have evidence of the role of such ion channels not only in the spike-to-burst firing pattern transition but also in the relation of such transition with the synchronous patterns. Furthermore, we can gain insights by examining situations where the channels are blocked selectively, rather than all simultaneously.

Supplementary Materials: The following supporting information can be downloaded at <https://www.mdpi.com/article/10.3390/brainsci13091347/s1>, Figure S1: Model of regular spiking neuron, with I_M , I_T , and I_L ; Figure S2: Firing pattern for different I_M and I_L conductances; Figure S3: Changes in network firing pattern with input current (I) and chemical synaptic conductance (g_{syn}); Figure S4: Dynamics of ionic currents in a neuron during the bistable regime.

Author Contributions: F.S.B., P.R.P. and R.F.O.P.: Conceived the work. F.S.B., P.R.P., C.F.B. and S.D.-B.: Developed the codes. F.S.B., P.R.P., D.L.M.S., C.F.B., E.C.G., L.E.B., J.D.S.J., A.M.B., I.L.C., S.D.-B. and R.F.O.P.: Analyzed the simulations, discussed the results, wrote and corrected the manuscript. All authors have read and agreed to the published version of the manuscript.

Funding: The authors acknowledge the financial support from São Paulo Research Foundation (FAPESP, Brazil) (Grants N. 2018/03211-6, 2020/04624-2, 2021/12232-0, 2022/13761-9), Fundação Araucária, CNPq, Coordenação de Aperfeiçoamento de Pessoal de Nível Superior—Brasil (CAPES), and NIH U24EB028998.

Institutional Review Board Statement: Not applicable.

Informed Consent Statement: Not applicable.

Data Availability Statement: Numerical simulations and analyses were implemented using custom C and Python code, using the NetPyNE modeling tool and the NEURON simulation engine, and can be freely accessed in <https://github.com/FernandoSBorges/BistabilityHH> (accessed on 1 September 2023). Data can be made available upon request.

Conflicts of Interest: The authors declare no conflict of interest.

References

- Hodgkin, A.L.; Huxley, A.F. A quantitative description of membrane current and its application to conduction and excitation in nerve. *J. Physiol.* **1952**, *117*, 500–544. [\[CrossRef\]](#)
- Dalla Porta, L.; Barbero-Castillo, A.; Sanchez-Sanchez, J.M.; Sanchez-Vives, M.V. M-current modulation of cortical slow oscillations: Network dynamics and computational modeling. *PLoS Comput. Biol.* **2023**, *19*, e1011246. [\[CrossRef\]](#) [\[PubMed\]](#)
- Burke, K.J., Jr.; Bender, K.J. Modulation of ion channels in the axon: Mechanism and function. *Front. Cell. Neurosci.* **2019**, *13*, 221. [\[CrossRef\]](#)
- Ranjan, R.; Logette, E.; Marani, M.; Herzog, M.; Tâche, V.; Scantamburlo, E.; Buchillier, V.; Markram, H. A kinetic map of the homomeric voltage-gated potassium channel (Kv) family. *Front. Cell. Neurosci.* **2019**, *13*, 358. [\[CrossRef\]](#) [\[PubMed\]](#)
- Smith, R.S.; Walsh, C.A. Ion channel functions in early brain development. *Trends Neurosci.* **2020**, *43*, 103–114. [\[CrossRef\]](#) [\[PubMed\]](#)
- Bando, Y.; Ishibashi, M.; Yamagishi, S.; Fukuda, A.; Sato, K.; Orchestration of ion channels and transporters in neocortical development and neurological disorders. *Front. Neurosci.* **2022**, *16*, 827284. [\[CrossRef\]](#)
- Hou, P.; Du, X.; An, H. Editorial: Ion channels: Therapeutic targets for neurological disease. *Front. Mol. Neurosci.* **2021**, *14*, 797327. [\[CrossRef\]](#)
- Hübner, C.; Jentsch, T.J. Ion channel diseases. *Hum. Mol. Genet.* **2002**, *11*, 2435–2445. [\[CrossRef\]](#)
- Kecskes, M.; Peigneur, S.; Held, K. Editorial: Contribution of ion channels to neuropathologies. *Front. Cell Dev. Biol.* **2023**, *11*, 1179663. [\[CrossRef\]](#)
- Podlaski, W.F.; Seeholzer, A.; Groschner, L.N.; Miesencöck, G.; Ranjan, R.; Vogels, T.P. Mapping the function of neuronal ion channels in model and experiment. *eLife* **2017**, *6*, e22152. [\[CrossRef\]](#)
- Nayak, L.; Dasgupta, A.; Das, R.; Ghosh, K.; De, R.K. Computational neuroscience and neuroinformatics: Recent progress and resources. *J. Biosci.* **2018**, *43*, 1037–1054. [\[CrossRef\]](#) [\[PubMed\]](#)
- Mishra, A.; Majhi, S.K. A comprehensive survey of recent developments in neuronal communication and computational neuroscience. *J. Ind. Inf. Integration* **2019**, *13*, 40–54. [\[CrossRef\]](#)
- Barbulescu, R.; Mestre, G.; Oliveira, A.L.; Silveira, L.M. Learning the dynamics of realistic models of *C. elegans* nervous system with recurrent neural networks. *Sci. Rep.* **2023**, *13*, 467. [\[CrossRef\]](#)
- Cannon, R.C.; D'Alessandro, G. The ion channel inverse problem: Neuroinformatics meets biophysics. *PLoS Comput. Biol.* **2006**, *2*, e91. [\[CrossRef\]](#)
- Lin, C.-Y.; Chen, P.-H.; Lin, H.-H.; Huang, W.-M. U(1) dynamics in neuronal activities. *Sci. Rep.* **2022**, *12*, 17629. [\[CrossRef\]](#)

16. Hansen, M.; Protachevicz, P.R.; Iarosz, K.C.; Caldas, I.L.; Batista, A.M.; Macau, E.E. Dynamics of uncoupled and coupled neurons under external pulsed currents. *Chaos Solit. Fractals* **2022**, *155*, 11734. [[CrossRef](#)]
17. Izhikevich, E.M. *Dynamical Systems in Neuroscience*; MIT Press: Cambridge, MA, USA, 2007.
18. Borges, F.S.; Protachevicz, P.R.; Lameu, E.L.; Bonetti, R.C.; Iarosz, K.C.; Caldas, I.L.; Baptista, M.S.; Batista, A.M. Synchronous behaviour in network model based on human cortico-cortical connections. *Neural Netw.* **2017**, *90*, 074006.
19. Protachevicz, P.R.; Borges, R.R.; Reis, A.S.; Borges, F.S.; Iarosz, K.C.; Caldas, I.L.; Lameu, E.L.; Macau, E.E.N.; Viana, R.L.; Sokolov, I.M.; et al. Synchronous behaviour in network model based on human cortico-cortical connections. *Physiol. Meas.* **2018**, *39*, 7. [[CrossRef](#)]
20. Jiao, X.; Wang, R. Synchronous firing patterns of neuronal population with excitatory and inhibitory connections. *Int. J. Non Linear Mech.* **2010**, *45*, 647–651. [[CrossRef](#)]
21. Wang, H.; Ma, J.; Chen, Y.; Chen, Y. Effect of an autapse on the firing pattern transition in a bursting neuron. *Commun. Nonlinear Sci. Numer. Simul.* **2014**, *19*, 3242–3254. [[CrossRef](#)]
22. Santos, M.S.; Protachevicz, P.R.; Iarosz, K.C.; Caldas, I.L.; Viana, R.L.; Borges, F.S.; Ren, H.-P.; Szezech, J.D.; Batista, A.M.; Grebogi, C. Spike-burst chimera states in an adaptive exponential integrate-and-fire neuronal network. *Chaos* **2019**, *29*, 4. [[CrossRef](#)]
23. Protachevicz, P.R.; Iarosz, K.C.; Caldas, I.L.; Antonopoulos, C.G.; Batista, A.M.; Kurths, J. Influence of autapses on synchronization in neural networks with chemical synapses. *Front. Syst. Neurosci.* **2020**, *14*, 604563. [[CrossRef](#)]
24. Protachevicz, P.R.; Hansen, M.; Iarosz, K.C.; Caldas, I.L.; Batista, A.M.; Kurths, J. Emergence of neuronal synchronization in coupled areas. *Front. Comput. Neurosci.* **2021**, *15*, 663408. [[CrossRef](#)]
25. Pena, R.F.O.; Lima, V.; Shimoura, R.O.; Paulo Novato, J.; Roque, A.C. Optimal Interplay between Synaptic Strengths and Network Structure Enhances Activity Fluctuations and Information Propagation in Hierarchical Modular Networks. *Brain Sci.* **2020**, *10*, 228. [[CrossRef](#)]
26. Huang, S.; Zhang, J.; Wang, M.; Hu, C.-H. Firing patterns transitions and desynchronization induced by time delay in neural networks. *Physica A* **2018**, *499*, 88–97. [[CrossRef](#)]
27. Protachevicz, P.R.; Borges, F.S.; Iarosz, K.C.; Baptista, M.S.; Lameu, E.L.; Hansen, M.; Caldas, I.L.; Szezech, J.D., Jr.; Batista, A.M.; Kurths, J. Influence of delayed conductance on neuronal synchronization. *Front. Physiol.* **2020**, *11*, 1053. [[CrossRef](#)] [[PubMed](#)]
28. Pena, R.F.O.; Zaks, M.A.; Roque, A.C. Dynamics of spontaneous activity in random networks with multiple neuron subtypes and synaptic noise. *J. Comput. Neurosci.* **2018**, *45*, 1–28. [[CrossRef](#)]
29. Protachevicz, P.R.; Bonin, C.A.; Iarosz, K.C.; Caldas, I.L.; Batista, A.M. Large coefficient of variation of inter-spike intervals induced by noise current in the resonate-and-fire model neuron. *Cogn. Neurodyn.* **2022**, *16*, 1461–1470. [[CrossRef](#)]
30. Protachevicz, P.R.; Santos, M.S.; Seifert, E.G.; Gabrick, E.C.; Borges, F.S.; Borges, R.R.; Trobia, J.; Szezech, J.D., Jr.; Iarosz, K.C.; Caldas, I.L.; et al. Noise induces continuous and non-continuous transitions in neuronal interspike interval range. *Indian Acad. Sci. Conf. Ser.* **2020**, *3*, 1.
31. Lowet, E.; Sheehan, D.J.; Chialva, U.; Pena, R.D.O.; De Mount, R.A.; Xiao, S.; Zhou, S.L.; Tseng, H.; Gritton, H.; Shroff, S.; et al. Theta and gamma rhythmic coding through two spike output modes in the hippocampus during spatial navigation. *Cell Rep.* **2023**, *42*, 112906. [[CrossRef](#)] [[PubMed](#)]
32. Gu, H.; Pan, B.; Xu, J. Experimental observation of spike, burst, and chaos synchronization of calcium concentration oscillations. *Europhys. Lett.* **2014**, *106*, 50003. [[CrossRef](#)]
33. Árhem, P.; Klement, G.; Blomberg, C. Channel density regulation of firing patterns in a cortical neuron model. *Biophys. J.* **2006**, *90*, 4392–4404. [[CrossRef](#)] [[PubMed](#)]
34. Protachevicz, P.R.; Borges, F.S.; Lameu, E.L.; Ji, P.; Iarosz, K.C.; Kihara, A.L.; Caldas, I.L.; Szezech, J.D., Jr.; Baptista, M.S.; Macau, E.E.N.; et al. Bistable firing patterns in a neural network model. *Front. Comput. Neurosci.* **2019**, *13*, 19. [[CrossRef](#)] [[PubMed](#)]
35. Cooper, D.C.; Chung, S.; Spruston, N. Output-mode transitions are controlled by prolonged inactivation of sodium channels in pyramidal neurons of subiculum. *PLoS Biol.* **2005**, *3*, e175. [[CrossRef](#)]
36. Wang, L.; Wang, Y.; Fu, W.-L.; Cao, L.-H. Modulation of neuronal dynamic range using two different adaptation mechanisms. *Neural Regen. Res.* **2017**, *12*, 3. [[CrossRef](#)]
37. Benda, J. Neural adaptation. *Curr. Biol.* **2021**, *31*, R110–R116. [[CrossRef](#)]
38. Trinh, A.; Girardi-Schappo, M.; Béique, J.; Longtin, A.; Maler, L. Dentate gyrus mossy cells exhibit sparse coding via adaptive spike threshold dynamics. *bioRxiv* **2022**, bioRxiv483263.
39. Ha, G.E.; Cheong, E. Spike frequency adaptation in neuron of the central nervous system. *Exp. Neurobiol.* **2017**, *26*, 179. [[CrossRef](#)]
40. Pospischil, M.; Toledo-Rodriguez, M.; Monier, C.; Piwkowska, Z.; Bal, T.; Frégnac, Y.; Destexhe, A. Minimal Hodgkin–Huxley type models for different classes of cortical and thalamic neurons. *Biol. Cybern.* **2008**, *99*, 427–441. [[CrossRef](#)]
41. Wang, J.; Deng, B.; Gao, T.; Jiang, W.; Hong, T. Spike-frequency adaptation inhibits the pairwise spike correlation. *Front. Neurosci.* **2023**, *17*, 1193930. [[CrossRef](#)]
42. Berger, S.D.; Crook, S.M. Modeling the influence of ion channels on neuron dynamics in *Drosophila*. *Front. Comput. Neurosci.* **2015**, *9*, 139. [[CrossRef](#)] [[PubMed](#)]
43. Lu, T.; Wade, K.; Hong, H.; Sanchez, J.T. Ion channel mechanisms underlying frequency-firing patterns of the avian nucleus mesencephalic: A computational model. *Channels* **2017**, *11*, 444–458. [[CrossRef](#)] [[PubMed](#)]
44. Landisman, C.E.; Long, M.A.; Beierlein, M.; Deans, M.R.; Paul, D.L.; Connors, B.W. Electrical synapses in the thalamic reticular nucleus. *J. Neurosci.* **2002**, *22*, 1002–1009. [[CrossRef](#)] [[PubMed](#)]

45. Svirskis, G.; Rinzel, J. Influence of temporal correlation of synaptic input on the rate and variability of firing in neurons. *Biophys. J.* **2000**, *79*, 629–637. [[CrossRef](#)] [[PubMed](#)]
46. Borges, F.S.; Moreira, J.V.S.; Takarabe, L.M.; Lytton, W.W.; Dura-Bernal, S. Large-scale biophysically detailed model of somatosensory thalamocortical circuits in NetPyNE. *Front. Neuroinform.* **2022**, *16*, 884245. [[CrossRef](#)]
47. Lu, Q.; Yang, Z.; Duan, L.; Gu, H.; Ren, W. Dynamics and transitions of firing patterns in deterministic and stochastic neuronal systems. *Chaos Solit. Fractals* **2009**, *40*, 577–597. [[CrossRef](#)]
48. Maisel, B.; Lindenberg, K. Channel noise effects on neural synchronization. *Phys. A Stat. Mech. Appl.* **2020**, *552*, 123186. [[CrossRef](#)]
49. Schmid, G.; Goychuk, I.; Hänggi, P. Channel noise and synchronization in excitable membranes. *Phys. A Stat. Mech. Appl.* **2003**, *325*, 165–175. [[CrossRef](#)]
50. Boaretto, B.R.R.; Manchein, C.; Prado, T.L.; Lopes, S.R. The role of individual neuron ion conductance in the synchronization processes of neuron networks. *Neural Netw.* **2021**, *137*, 97–105. [[CrossRef](#)]
51. Ladenbauer, J.; Augustin, M.; Shiau, L.; Obermayer, K. Impact of adaptation currents on synchronization of coupled exponential integrate-and-fire neurons. *PLoS Comput. Biol.* **2012**, *8*, e1002478. [[CrossRef](#)]
52. Avoli, M. Mechanism of epileptiform synchronization in cortical neuronal networks. *Curr. Med. Chem.* **2014**, *21*, 653–662. [[CrossRef](#)]
53. Traub, R.D.; Wong, R.K.S. Cellular mechanism of neuronal synchronization in epilepsy. *Science* **1982**, *216*, 745–747. [[CrossRef](#)] [[PubMed](#)]
54. Hofer, K.T.; Kandrás, A.; Tóth, K.; Hajnal, B.; Bokodi, V.; Tóth, E.Z.; Efos, L.; Entz, L.; Bagó, A.G.; Fabó, D.; et al. Bursting of excitatory cells is linked to interictal epileptic discharge generation in humans. *Nature* **2022**, *12*, 6280. [[CrossRef](#)] [[PubMed](#)]
55. Jiruska, P.; de Curtis, M.; Jefferys, J.G.; Schevon, C.A.; Schiff, S.J.; Schindler, K. Synchronization and desynchronization in epilepsy: Controversies and hypotheses. *J. Physiol.* **2013**, *591*, 787–797. [[CrossRef](#)]
56. Chen, C.; Chen, L.; Lin, Y.; Zeng, S.; Luo, Q. The origin of spontaneous synchronized burst in cultured neuronal networks based on multi-electrode arrays. *Biosystems* **2006**, *85*, 137–143. [[CrossRef](#)]
57. Matsumoto-Makidono, Y.; Nakayama, H.; Yamasaki, M.; Miyazaki, T.; Kobayashi, K.; Watanabe, M.; Hashimoto, K. Ionic basis for membrane potential resonance in neurons of the inferior olive. *Cell Rep.* **2016**, *16*, 994–1004. [[CrossRef](#)] [[PubMed](#)]
58. Graef, J.; Nordskog, B.K.; Wiggins, W.F.; Godwin, S.W. An acquired channelopathy involving thalamic T-type Ca^{2+} channels after status epilepticus. *J. Neurosci.* **2009**, *29*, 4430–4441. [[CrossRef](#)]
59. Becker, A.J.; Pitsch, J.; Sochivko, D.; Opitz, T.; Staniek, M.; Chen, C.-C.; Campbell, K.P.; Schoch, S.; Yaari, Y.; Beck, H. Transcriptional upregulation of Cav3.2 mediates epileptogenesis in pilocarpine model of epilepsy. *J. Neurosci.* **2008**, *28*, 13341–13353. [[CrossRef](#)]
60. Su, H.; Sochivko, D.; Becker, A.; Chen, J.; Jiang, Y.; Yaari, Y.; Becker, H. Upregulation of a T-type Ca^{2+} channel causes a long-lasting modification of neuronal firing mode after status epilepticus. *J. Neurosci.* **2002**, *22*, 3645–3655. [[CrossRef](#)]
61. Dovzhenok, A.; Kuznetsov, A.S. Exploring neuronal bistability at the depolarization block. *PLoS ONE* **2012**, *7*, e42811. [[CrossRef](#)]
62. Tartaglia, E.M.; Brunel, N. Bistability and up/down state alternations in inhibition-dominated randomly connected networks of LIF neurons. *Sci. Rep.* **2017**, *7*, 11916. [[CrossRef](#)] [[PubMed](#)]
63. Compte, A.; Sanchez-Vives, M.V.; McCormick, D.A.; Wang, X.-J. Cellular and Network Mechanism of slow oscillatory activity (1< Hz) and wave propagation in a cortical network model. *J. Neurophysiol.* **2003**, *89*, 5.
64. Boaretto, B.R.R.; Budzinski, R.C.; Rossi, K.L.; Manchein, C.; Prado, T.L.; Feudel, U.; Lopes, S.R. Bistability in synchronization of identical neurons. *Phys. Rev. E* **2021**, *104*, 0240204. [[CrossRef](#)] [[PubMed](#)]
65. Akcay, Z.; Xinxian, H.; Nadim, F.; Bose, A. Phase-locking and bistability in neuronal networks with synaptic depression. *Phys. D Nonlinear Phenom.* **2018**, *364*, 8–21. [[CrossRef](#)]
66. Lu, Y.; Xin, X.; Rinzel, J. Bistability at the onset of neuronal oscillations. *Biol. Cybern.* **2023**, *117*, 61–79. [[CrossRef](#)]
67. Fröhlich, F.; Bazhenov, M. Coexistence of tonic firing and bursting in cortical neurons. *Phys. Rev. E* **2006**, *74*, 031922. [[CrossRef](#)]
68. Meng, J.H.; Riecke, H. Synchronization by uncorrelated noise: Interacting rhythms in interconnected oscillator networks. *Sci. Rep.* **2018**, *8*, 6949. [[CrossRef](#)]
69. Kelso, J.A.S. Multistability and metastability: Understanding dynamic coordination in the brain. *Philos. Trans. R. Soc. B Biol. Sci.* **2012**, *367*, 906–918. [[CrossRef](#)]
70. Silva, F.L.; Blanes, W.; Kalitzin, S.N.; Parra, J.; Suffczynski, P.; Velos, D.N. Epilepsies as dynamical diseases of brain systems: Basic models of the transition between normal and epileptic activity. *Epilepsia* **2003**, *44*, 72–83. [[CrossRef](#)]
71. Dayan, P.; Abbott, L.F. *Theoretical Neuroscience: Computational and Mathematical Modeling of Neural*; MIT Press: Cambridge, MA, USA, 2005; pp. 160–162.
72. Traub, R.D.; Miles, R. *Neuronal Networks of the Hippocampus*; Cambridge University Press: Cambridge, UK, 1991.
73. Yamada, W.M.; Koch, C.; Adams, P.R. *Multiple Channels and Calcium Dynamics, Methods in Neuronal Modeling: From Synapses to Networks*; MIT Press: Cambridge, MA, USA, 1989; pp. 97–134.
74. Destexhe, A.; Neubig, M.; Ulrich, D.; Huguenard, J. Dendritic low-threshold calcium currents in thalamic relay cells. *J. Neurosci.* **1998**, *18*, 3574–3588. [[CrossRef](#)]
75. Reuveni, I.; Friedman, A.; Amitai, Y.; Gutnick, M.J. Stepwise repolarization from Ca^{2+} plateaus in neocortical pyramidal cells: Evidence for nonhomogeneous distribution of HVA Ca^{2+} channels in dendrites. *J. Neurosci.* **1993**, *13*, 4609–4621. [[CrossRef](#)] [[PubMed](#)]

76. Destexhe, A.; Bal, T.; McCormick, D.A.; Sejnowski, T.J. Ionic mechanisms underlying synchronized oscillations and propagating waves in a model of ferret thalamic slices. *J. Neurophysiol.* **1996**, *76*, 2049–2070. [[CrossRef](#)] [[PubMed](#)]
77. Huguenard, J.R.; McCormick, D.A. Simulation of the currents involved in rhythmic oscillations in thalamic relay neurons. *J. Neurophysiol.* **1992**, *68*, 1373–1383. [[CrossRef](#)]
78. Noback, C.R.; Ruggiero, D.A.; Strominger, N.L.; Demarest, R.J. *The Human Nervous System: Structure and Function*; Springer Science & Business Media: Berlin/Heidelberg, Germany, 2005; p. 744.
79. Borges, F.S.; Protachevitz, P.R.; Pena, R.F.O.; Lameu, E.L.; Higa, G.S.V.; Kihara, A.H.; Matias, F.S.; Antonopoulos, C.G.; de Pasquale, R.; Roque, A.C.; et al. Self-sustained activity of low firing rate in balanced networks. *Phys. A Stat. Mech. Appl.* **2020**, *537*, 122671. [[CrossRef](#)]
80. Kuramoto, Y. *Chemical Oscillations, Waves, and Turbulence*; Springer: Berlin/Heidelberg, Germany, 1984.
81. Hansen, M.; Protachevitz, P.R.; Iarosz, K.C.; Caldas, I.L.; Batista, A.M.; Macau, E.E.N. The effect of time delay for synchronisation suppression in neuronal networks. *Chaos Solit. Fractals* **2022**, *164*, 112690. [[CrossRef](#)]
82. Dura-Bernal, S.; Suter, B.A.; Gleeson, P.; Cantarelli, M.; Quintana, A.; Rodriguez, F.; Kedziora, D.J.; Chadderdon, F.L.; Kerr, C.C.; Neymotin, S.A.; et al. NetPyNE, a tool for data-driven multiscale modeling of brain circuits. *eLife* **2019**, *8*, e44494.
83. Vijayan, S.; Hale, G.J.; Moore, C.I.; Brown, E.N.; Wilson, M. Activity in the barrel cortex during active behavior and sleep. *J. Neurophysiol.* **2010**, *103*, 2074–2084. [[CrossRef](#)]
84. Borges, F.S.; Gabrick, E.C.; Protachevitz, P.R.; Higa, G.S.V.; Lameu, E.L.; Rodriguez, P.X.R.; Ferraz, M.S.A.; Szezech, J.D.; Batista, A.M.; Kihara, A.H. Intermittency properties in a temporal lobe epilepsy model. *Epilepsy Behav.* **2023**, *139*, 109072. [[CrossRef](#)]
85. Alonso, L.M.; Marder, E. Visualization of currents in neural models with similar behavior and different conductance densities. *eLife* **2019**, *8*, e42722. [[CrossRef](#)]
86. Eun, S.H.; Kim, H.D.; Eun, B.L.; Lee, I.K.; Chung, H.J.; Kim, J.S.; Kang, H.C.; Lee, Y.M.; Suh, E.S.; Kim, D.W.; et al. Comparative trial of low- and high-dose zonisamide as monotherapy for childhood epilepsy. *Seizure* **2011**, *20*, 558–563. [[CrossRef](#)]
87. Zhang, S.; Zhu, Y.; Cheng, J.; Tao, J. Ion channels in epilepsy: Blasting fuse for neuronal hyperexcitability. In *Epilepsy—Advances in Diagnosis and Therapy*; Al-Zwaini, I.J., Albadri, B.A.-H., Eds.; IntechOpen: London, UK, 2018; Chapter 10.
88. Palmer, E.E. Potassium channel mutations in epilepsy. In *The Oxford Handbook of Neuronal Ion Channels*; Bhattacharjee, A., Ed.; Oxford University Press: Oxford, UK, 2018.
89. Chen, X.; Feng, Y.; Quinn, R.J.; Pountney, D.L.; Richardson, D.R.; Mellick, G.D.; Ma, L. Potassium Channels in Parkinson's Disease: Potential Roles in Its Pathogenesis and Innovative Molecular Targets for Treatment. *Pharmacol. Rev.* **2023**, *75*, 758–788.
90. Xu, J.-H.; Tang, F.-R. Voltage-dependent calcium channels, calcium binding proteins, and their interaction in the pathological process of epilepsy. *Int. J. Mol. Sci.* **2018**, *19*, 2735. [[CrossRef](#)]
91. Jorge, B.S.; Campbell, C.M.; Miller, A.R.; Kearney, J.A. Voltage-gated potassium channel KCNV2 (Kv8.2) contributes to epilepsy susceptibility. *Proc. Natl. Acad. Sci. USA* **2011**, *108*, 5443–5448. [[CrossRef](#)] [[PubMed](#)]
92. Zamponi, G.W.; Lory, P.; Perez-Reyes, E. Role of voltage-gate calcium channels in epilepsy. *Neuroscience* **2010**, *460*, 395–403.
93. Zamponi, G.W.; Striessnig, J.; Koschak, A.; Dolphin, A.C. The physiology, and pharmacology of voltage-gated calcium channels and their future therapeutic potential. *Pharmacol. Rev.* **2015**, *67*, 821–870. [[PubMed](#)]
94. Han, D.-Y.; Guan, B.-J.; Wang, Y.-J.; Hatzoglou, M.; Mu, T.-W. L-type calcium channel blockers enhance trafficking and function of epilepsy-associated $\alpha 1$ (D219N) subunits of GABA_A receptors. *J. Am. Chem. Soc.* **2015**, *137*, 2135–2148. [[CrossRef](#)] [[PubMed](#)]
95. Köhling, R.; Wolfart, J. Potassium channels in Epilepsy. *Cold Spring Harb. Perspect. Med.* **2016**, *6*, a022871. [[CrossRef](#)] [[PubMed](#)]
96. Passmore, G.M.; Reilly, J.M.; Thakur, M.; Keasberry, V.N.; Marsh, S.J.; Dickenson, A.H.; Brown, D.A. Functional significance of M-type potassium channels in nociceptive cutaneous sensory endings. *Front. Mol. Neurosci.* **2012**, *5*, 63. [[CrossRef](#)]
97. Cooper, E.C. Potassium Channels (including KCNQ) and Epilepsy. In *Jasper's Basic Mechanisms of the Epilepsies*, 4th ed.; Noebels, J.L., Avoli, M., Rogawski, M.A., Olsen, R., Delgado-Escueta, A.V., Eds.; National Center for Biotechnology Information (US): Bethesda, MD, USA, 2012.
98. Humphries, E.S.A.; Dart, C. Neuronal and cardiovascular Potassium channels as therapeutic drug targets: Promise and pitfalls. *J. Biomol. Screen.* **2015**, *20*, 1055–1073.
99. Niday, Z.; Tzingounis, A.V. Potassium channel gain of function in epilepsy: An unresolved paradox. *Neuroscientist* **2018**, *24*, 368–380.
100. Villa, C.; Combi, R. Potassium channels and human epileptic phenotypes: An updated overview. *Front. Cell. Neurosci.* **2016**, *10*, 81. [[CrossRef](#)] [[PubMed](#)]
101. McCoy, M.T.; Jayanthi, S.; Cadet, J.L. Potassium channels and their potential roles in substance use disorders. *Int. J. Mol. Sci.* **2021**, *22*, 1249. [[CrossRef](#)] [[PubMed](#)]
102. Gao, K.; Lin, Z.; Wen, S.; Jiang, Y. Potassium channels and epilepsy. *Acta Neurol. Scand.* **2022**, *146*, 699–707. [[CrossRef](#)] [[PubMed](#)]
103. Smart, S.L.; Lopantsev, V.; Zhang, C.L.; Robbins, C.A.; Wang, H.; Chiu, S.Y.; Schwartzkroin, P.A.; Messing, A.; Tempel, B.L. Deletion of the K_v1.1 Potassium channel causes epilepsy in mice. *Neuron* **1998**, *20*, 809–819. [[CrossRef](#)]
104. Ågren, R.; Nilsson, J.; Århem, P. Closed and open state dependent block of potassium channels cause opposing effects on excitability—A computational approach. *Sci. Rep.* **2019**, *9*, 8175. [[CrossRef](#)]
105. Rajakulendran, S.; Hanna, M.G. The role of calcium channels in epilepsy. *Cold Spring Harb. Perspect. Med.* **2016**, *6*, a022723. [[CrossRef](#)]

106. Powell, K.L.; Cain, S.M.; Snutch, T.P.; O'Brien, T.J. Low threshold T-type calcium channels as targets for novel epilepsy treatments. *Br. J. Clin. Pharmacol.* **2013**, *77*, 729–739. [[CrossRef](#)]
107. Roopa, B.; Janardhan, M.; Karunasree, P. Effect of calcium blocker as anticonvulsant and its potentiating effect when used along with sodium valproate in pentylenetetrazole induced seizures in Albino rats. *Int. J. Basic Clin. Pharmacol.* **2008**, *7*, 714.
108. Willmore, L.J. Calcium antagonists and epilepsy. *Mayo Clin. Proc.* **1995**, *80*, 70–715. [[CrossRef](#)]
109. Tringham, E.; Powell, K.L.; Cain, S.M.; Kuplast, K.; Mezeyoya, J.; Weerapura, M.; Eduljee, C.; Jiang, X.; Smith, P.; Morrison, J.-L.; et al. T-Type calcium channel blockers that attenuate thalamic burst firing and suppress absense seizures. *Epilepsy* **2012**, *4*, 121.
110. Kulak, W.; Sobaniec, W.; Wojtal, K.; Czuczwar, S.J. Calcium modulation in epilepsy. *Pol. J. Pharmacol.* **2004**, *56*, 29–41. [[PubMed](#)]
111. Kopecky, B.J.; Liang, R.; Bao, J. T-type calcium channel blockers as neuroprotective agents. *Pflug. Arch. Eur. J. Physiol.* **2014**, *466*, 757–765. [[CrossRef](#)] [[PubMed](#)]
112. Cain, S.M.; Snutch, T.P. T-type calcium channels in burst-firing, network synchrony, and epilepsy. *Biochim. Biophys. Acta* **2018**, *1828*, 1572–1578. [[CrossRef](#)]
113. El-Azab, M.F.; Moustafa, Y.M. Influence of calcium channel blockers on anticonvulsant and antinociceptive activities of valproic acid in pentylenetetrazole-kindled mice. *Pharmacol. Rep.* **2012**, *64*, 305–314. [[CrossRef](#)] [[PubMed](#)]
114. Gardos, G. The function of calcium in the potassium permeability of human erythrocytes. *Biochim. Biophys. Acta Bioenerg.* **1958**, *30*, 653–654. [[CrossRef](#)] [[PubMed](#)]
115. Hille, B. Ionic channels in excitable membranes. Current problems and biophysical approaches. *Biophys. J.* **1978**, *22*, 283–294. [[CrossRef](#)]
116. Vergara, C.; Latorre, R.; Marrion, N.V.; Adelman, J.P. Calcium-activated potassium channels. *Curr. Opin. Neurobiol.* **1998**, *8*, 321–329. [[CrossRef](#)]
117. Momin, A.; Cadiou, H.; Mason, A.; McNaughton, P.A. Role of the hyperpolarization-activated current I_h in somatosensory neurons. *J. Physiol.* **2008**, *586*, 5911–5929. [[CrossRef](#)]
118. Stafstrom, C.E. Persistent sodium current and its role in epilepsy. *Epilepsy Curr.* **2007**, *7*, 15–22. [[CrossRef](#)]

Disclaimer/Publisher's Note: The statements, opinions and data contained in all publications are solely those of the individual author(s) and contributor(s) and not of MDPI and/or the editor(s). MDPI and/or the editor(s) disclaim responsibility for any injury to people or property resulting from any ideas, methods, instructions or products referred to in the content.